energies

MDPI

Article

Effect of the Air Flow on the Combustion Process and Preheating Effect of the Intake Manifold Burner

Zhishuang Li, Ziman Wang *, Haoyang Mo and Han Wu

School of Mechanical Engineering, Beijing Institute of Technology, Beijing 100081, China; wulixue080@163.com (Z.L.); mohaoyang163@163.com (H.M.); hwu@bit.edu.cn (H.W.)
* Correspondence: ziman.wang@bit.edu.cn; Tel.: +86-010-6891-8581

Abstract: Diesel engines show poor performance and high emissions under cold-start conditions. The intake manifold burner is an effective method to increase the intake air temperature and improve engine performance. In this paper, a visualization system was employed to investigate the combustion process of the intake manifold burner. The effects of diesel flow rate and airflow velocity on combustion performance were investigated. The combustion process of the intake manifold burner showed four stages: preparing stage A, rapid development stage B, steady-development stage C, and stable stage D. Flame stripping was found in stages C and D, presenting the instability of the combustion process. With the increase in air flow velocity from 1.4 m/s to 3.0 m/s, the flame stripping was enhanced, leading to the increasing combustion instability and regular flame penetration fluctuations. The average temperature rise and combustion efficiency increased with the increasing diesel flow rate, indicating the combustion enhancement. Comparison of temperature rise and combustion efficiency under 2.0 m/s and 10.0 m/s showed that stronger cross wind enhances the heat convection, improving the temperature uniformity and combustion efficiency.

Keywords: intake manifold burner; flame; instability; preheat; diesel engine; cold-start

Citation: Li, Z.; Wang, Z.; Mo, H.; Wu, H. Effect of the Air Flow on the Combustion Process and Preheating Effect of the Intake Manifold Burner. *Energies* **2022**, *15*, 3260. https://doi.org/10.3390/en15093260

Academic Editors: Haifeng Liu, Zongyu Yue and Constantine D. Rakopoulos

Received: 7 March 2022
Accepted: 7 April 2022
Published: 29 April 2022

1. Introduction

The application of diesel engines greatly affects our daily life, for instance, through transportation and power generation. Compared with a gasoline engine, a diesel engine shows lower CO_2 emission on urban and motorway [1]. Environment protection is one of the most important worldwide topics. Diesel engine still faces enormous challenges to meet the requirements of worldwide environmental problems and human health. In order to obtain better engine performance, different methods such as split injection strategy [2,3], biodiesel [4], emulsified fuels [5], and oxygen-enriched combustion [6] have been used to improve the spray breakup, combustion efficiency, and emissions. Though improved by various methods, the emission and performance of diesel engines under the sub-zero environment remains a critical problem.

Under the low-temperature environment, diesel engine shows poor performance and high emissions. The skip-cycle (misfire) number increased with the decreasing ambient temperature [7]. A significant increase in the white smoke emissions and starting time was shown when the ambient temperature reduced from −5 °C to −20 °C [8]. It was found that CO and HC emission showed a rapid increase after the engine-start at a low temperature due to the incomplete combustion [9]. The CO, PM, and HC emissions under cold-start conditions were much higher than those of warm-start, especially during the first 30 s [10]. With the ambient temperature increasing from −20 °C to 20 °C, the fuel injection quantity and NOx and HC emissions decreased significantly [11]. Higher intake temperature led to lower soot emissions and shorter ignition delay [12]. During the warm-up process from cold-start, the modern tier-4 turbo-charged diesel engine showed decreased NOx emissions [13]. Ko et al. [9] found that the hydrocarbon emissions of CH_4, C_2H_4, and C_3H_6

increased several times under cold-start conditions because the thermal cranking process was affected by heat loss and high fuel-air equivalence ratios. Compared with the test under hot-start conditions, the oxygenated fuels under cold-start conditions showed a significant increase in NOx, PN, PM_1, and $PM_{2.5}$ emissions [14]. Park et al. [15] reported that the diesel density and kinematic viscosity increased with decreasing fuel temperature. With a single main injection strategy, though the diesel spray was ignited with the aid of a metallic glow plug at 253 K, poor combustion development ensued due to the low diesel vaporization [15].

Intake air heating strategy was found to effectively improve the engine performance and decrease the emissions. Rath et al. [16] investigated the effect of preheated air on a diesel engine and it was found that when the intake air preheat strategy was applied, the brake specific fuel consumption, the CO and HC emissions, and the smoke opacity decreased. Compared with the case at a low intake air temperature of −7 °C, the diesel engine under the temperature of 15 °C showed higher peak engine speed and lower injected fuel, hydrocarbon, NOx, and particle emissions [17]. Dardiotis et al. [18] investigated the emissions of diesel cars and found that when compared with the test at 22 °C, the diesel vehicles at −7 °C showed higher HC, CO, and NOx emission over the urban driving cycle. In the diesel methanol dual fuel engine, the methanol, formaldehyde, NO_2, HC, and CO emissions decreased with the increasing intake air temperature while the total NOx emissions increased [19]. Yontar et al. [20] reported the intake air temperature effect for HCCI engine with the hydrogen-enriched kerosene-DME mixture as fuel. This study reported that as the intake air temperature increased from 273 K to 373 K, the CO, HC, and soot emission decreased while the maximum heat release rate, the brake specific fuel consumption, and the NOx emission increased.

Strategies were studied to preheat the intake air temperature. Broatch et al. [21] pointed out that both the engines with high and low compression ratios required a preheating strategy at the ambient temperature of −23 °C. The glow plug surface temperature required for successful ignition increased with the decreasing bulk gas temperature [22]. Celik et al. [23,24] preheated the intake air through the vortex tube, decreasing the fuel consumption and PM emissions. The intake air could also be preheated by using the heat energy of the exhaust gas [16]. Deng et al. [25] tested the influence of electrical intake air heater on cold-start performance by simulation and experiments and pointed out that a longer preheat time was needed at the low cold-start temperature. Preheated intake air boosted the fuel vaporization and tended to reduce the HC and CO emissions [26]. The electric starting heater was found to decrease the cranking time and energy consumption [27]. When the intake air temperature was preheated by the electrical intake air heater, a better effect on decreasing HC and CO emissions was reported in comparison with glow plugs [28]. The noise level decreased with the increasing intake air temperature due to the reduced ignition delay and the resultant decreased pressure rise rate [28]. When the same electrical energy of glow plugs was used, the electrical intake air heater showed a longer starting time but better speed stability after starting [29]. The intake manifold burner was found to provide sufficiently high air temperature, leading to a significant reduction in HC emission [30]. With the flame burner system employed as the starting aid, the starting time and white smoke emissions decreased significantly [8]. In [31], the minimum cranking time decreased to about 6 s. It was also found that the intake manifold burner (flame glow plug) was sufficient to preheat the intake air temperature up to the warm start conditions [30]. Sun et al. [32] studied the catalytic burner by igniting the recirculated exhaust gas (EGR). It was reported that with the catalytic burner assistance, the heavy-duty diesel engine was successfully started with the ambient temperature as low as −31.6 °C. With the intake manifold flame heater assisted starting, the intake charge dilution was shown and the effective equivalence ratio increased [33]. Zhang et al. [34] studied the cold-start performance of a diesel engine with the intake flame preheating strategy through simulation. They found that with the preheating strategy, the cold-start performance was greatly improved.

In the previous studies [8,23–34], the engine performance and exhaust emissions of the intake air preheating were covered. Although the intake manifold burner reduced the cross-sectional area of the intake air path, consumed the oxygen, and introduced the combustion product species into the cylinder, the intake air temperature and the engine performance were significantly improved [34]. In order to obtain the best performance, more detailed studies about the intake manifold burner are required. The ignition of the intake manifold burner is unstable and the combustion process still needs to be studied. Further investigation on the combustion of the intake manifold burner is essential to improve the engine performance. In the present study, the effects of the air flow velocity and diesel flow rate on the combustion process were studied. The flame stripping phenomenon was generated by the flame motion, leading to combustion instability. The ignition probability under different air flow velocities was investigated. The interactions between the flame motion and both the intake air flow and diesel flow rate were also probed. The preheating effect of the intake manifold burner was then evaluated by the temperature rise and the combustion efficiency.

2. Experiment Setup

Figure 1a shows the schematic of the intake manifold burner. The intake manifold burner consisted of two heating elements with a high surface temperature. Fuel was delivered into the intake manifold burner through the inlet port and evaporated by the heating elements. Then the gaseous fuel was ignited by the tips of heating elements.

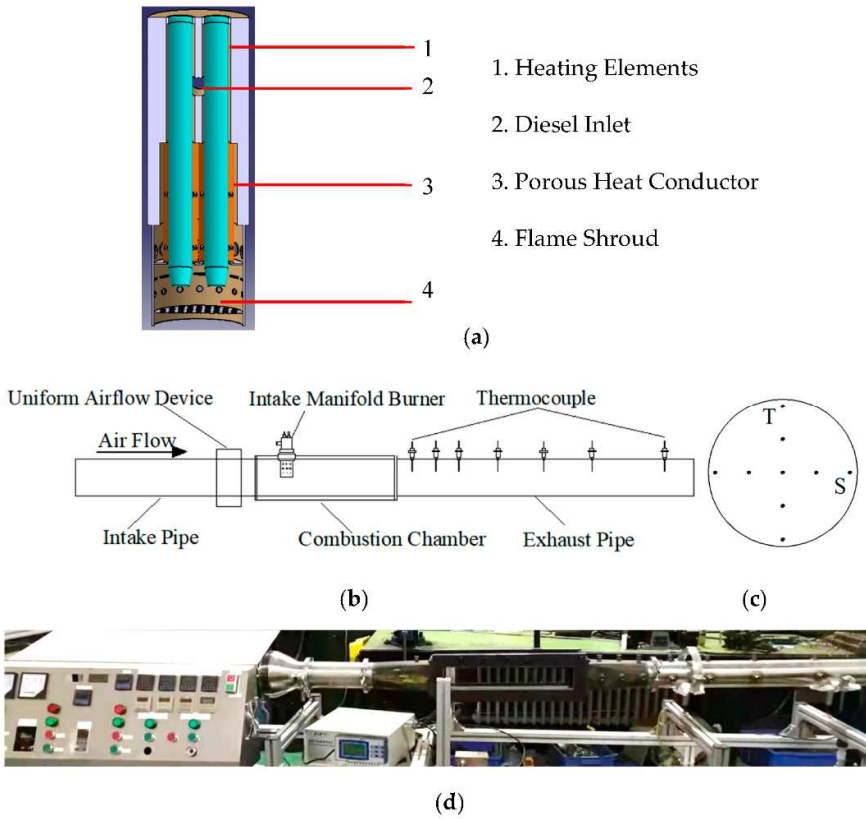

Figure 1. Schematic diagram of (**a**) the intake manifold burner, (**b**) the test system, and (**c**) the temperature measuring points in the cross-section of the exhaust pipe. (**d**) Photo of the test system.

The preheat system consisted of an intake pipe, intake manifold burner, combustion chamber, and exhaust pipe, as shown in Figure 1b. A powerful fan was used as the power source to provide the intake air flow. Through the "uniform air flow device" with evenly distributed small holes, the uniform intake air flow was obtained. Transparent quartz

windows of 80 × 500 mm^2 size were used in the combustion chamber, allowing the flame propagation process to be visualized. A high-speed camera (Phantom V7.3) was employed to capture the flame. The exposure time was set to 100 μs and the frame speed was set to 5000 fps due to the slow diffusion flame development. It took a long time to capture the whole combustion process. The intake manifold burner was cooled by the air flow after each experiment.

Thermocouples were installed along the axial direction on the exhaust pipe through the adjustable adapter, which allowed the depths of the thermocouple probes to be adjusted. Each cross-section had one thermocouple in the vertical and horizontal directions, which is marked with "T" and "S", respectively. The average temperature rise of every point was calculated by repeating the tests 5 times. The temperature measuring points in the cross-section of the exhaust pipe are shown in Figure 1c. In the cross-section, the temperature measured in the vertical and horizon directions is marked with "T" and "S", respectively. Air temperature at points of both sides with the distance of 0 mm, 20 mm, and 40 mm away from the circle center of the cross-section was measured, and the average temperature rise in the cross section of the exhaust pipe was calculated.

The measurement range of the K-type thermocouples was 0–1100 °C with an accuracy of 1%. The temperature rise is defined as follows:

$$\Delta T = T_1 - T_2 \quad (1)$$

where T_1 and T_2 are the air flow temperature before and after the combustion, respectively. Compared with the air flow temperature, the temperature difference could eliminate the measurement error and improve the accuracy. Moreover, the preheating effect could be obtained from the temperature rise of the air flow.

3. Test Fuel and Conditions

In this study, commercial diesel fuel was employed. The experiments were performed at atmospheric pressure. Both the fuel and ambient temperature were kept at 20 °C and the voltage was 24 V. Diesel was delivered to the intake manifold burner through a fuel pump to study the combustion process.

The effect of the diesel flow rate on combustion was studied with the fixed intake air flow velocity of 1.4 m/s and increasing diesel flow rate from 7.3 mL/min to 18.9 mL/min. The fuel flow rate was measured by the measuring cylinder with the known volume, and the average value of five repeating tests was employed to ensure the accuracy (1%). The influence of the intake air flow velocity was studied with the fixed diesel flow rate of 10.0 mL/min and increasing air flow velocity from 1.4 m/s to 3.0 m/s. The anemometer with a measurement range of 0–30.0 m/s and accuracy of 3% was used to measure the intake air flow velocity. The temperature increment under the air flow of 2.0 m/s and 10.0 m/s was measured to assess the preheating effect of the intake manifold burner on the intake air. The test conditions are shown in Table 1.

Table 1. Test conditions.

Conditions	Intake Air Flow Velocity (m/s)	Diesel Flow Rate (mL/min)	Air-Fuel Ratio
Combustion Process	1.4	7.3–18.9	134.5–51.95
	1.4–3.0	10.0	98.18–210.4
Temperature Rise	2.0	7.3–15.2	192.15–92.28
	10.0		960.75–461.4

The tests were repeated five times to get the combustion process and the ignition probability with different air flow velocities was repeated 10 times. The minimum preheat time needed for ignition was also obtained through the repeated experiments. The flame

penetration and flame area were calculated through an in-house built MATLAB script which was employed to identify the boundaries of flame in the combustion chamber.

4. Results and Discussion

4.1. Ignition Probability

Through the quartz windows of the combustion chamber, the combustion process was captured by the high-speed camera. When the power was supplied, the surface temperature of heating elements rose quickly. Liquid diesel was evaporated by the heating elements of the intake manifold burner. The gaseous diesel mixed with air in the flame shroud. Then, the fuel-air mixture could be ignited by the rod tips or not. All the cases were repeated 10 times and the proportion that the combustion happened was defined as the ignition probability, as shown below:

$$IP = N_1/N_2 \quad (2)$$

where N_1 is the number of success ignition and N_2 is the number of tests.

The ignition probability under different air flow velocities is shown in Figure 2. The ignition probability was carried out under the intake air flow of 1.4 m/s and the diesel flow rate of 7.3 mL/min. The intake manifold burner was powered on for tens of seconds, then diesel was injected into the burner. The preheating time that makes the ignition probability range from 0% to 100% was defined as "the starting time". The starting time at the air flow velocity of 3.6 m/s was from 19 s to 25 s. Compared with the case under 3.6 m/s, the starting time under 2.4 m/s was shorter, varying from 14 s to 17 s. With the increasing air flow velocity, more heat was carried away by the air flow due to stronger forced heat convention. Thus, more preheating time was needed to provide sufficient thermal heat for diesel evaporation and ignition.

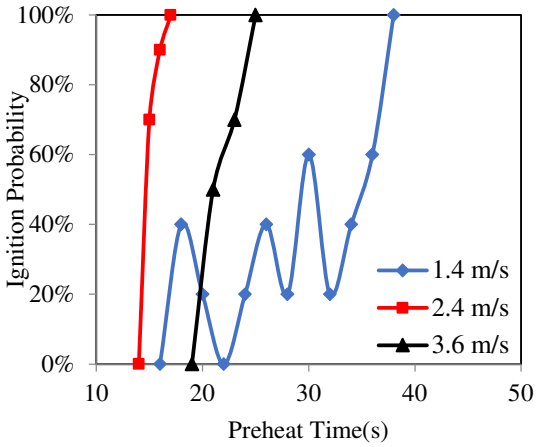

Figure 2. Ignition probability with different air flow velocities under the fuel flow rate of 7.3 mL/min.

The starting time under 1.4 m/s was from 16 s to 38 s, which was longer than that under the higher air flow velocity of 2.4 m/s and 3.6 m/s. The ignition probability increased gradually from 0% to 100% with the increasing preheat time under 2.4 m/s and 3.6 m/s, while the ignition probability under 1.4 m/s presented a complicated trend. With the decreasing air flow velocity, the reduction in oxygen concentration led to incomplete combustion. Therefore, the combustion probability was unstable and more preheat time was needed to ignite the diesel vapor under 1.4 m/s.

4.2. Flame Penetration

The whole process of combustion was divided into "the process before ignition" and the "combustion process". During the process before ignition, diesel flows into the flame shroud after the injection and it takes time to evaporate and mix with air. Then, the fuel-air mixture is ignited by the heating elements, entering the stage of the combustion process. The combustion process of the intake manifold burner was divided into four parts:

preparing stage A, rapid development stage B, steady-development stage C, and stable stage D, as shown in Figure 3. The intake manifold burner was powered on for 80 s before the injection of fuel. That is to say, when the fuel was injected into the burner, the rod's surface reached an ultra-high temperature that was sufficient to ignite the diesel vapor. The delay of flame penetration development is shown in stage A. During stage A, the flame located inside the intake manifold burner, which could be seen through the holes. The delay of flame development was thought to be caused by the accumulation of heat and diesel evaporation in the flame shroud.

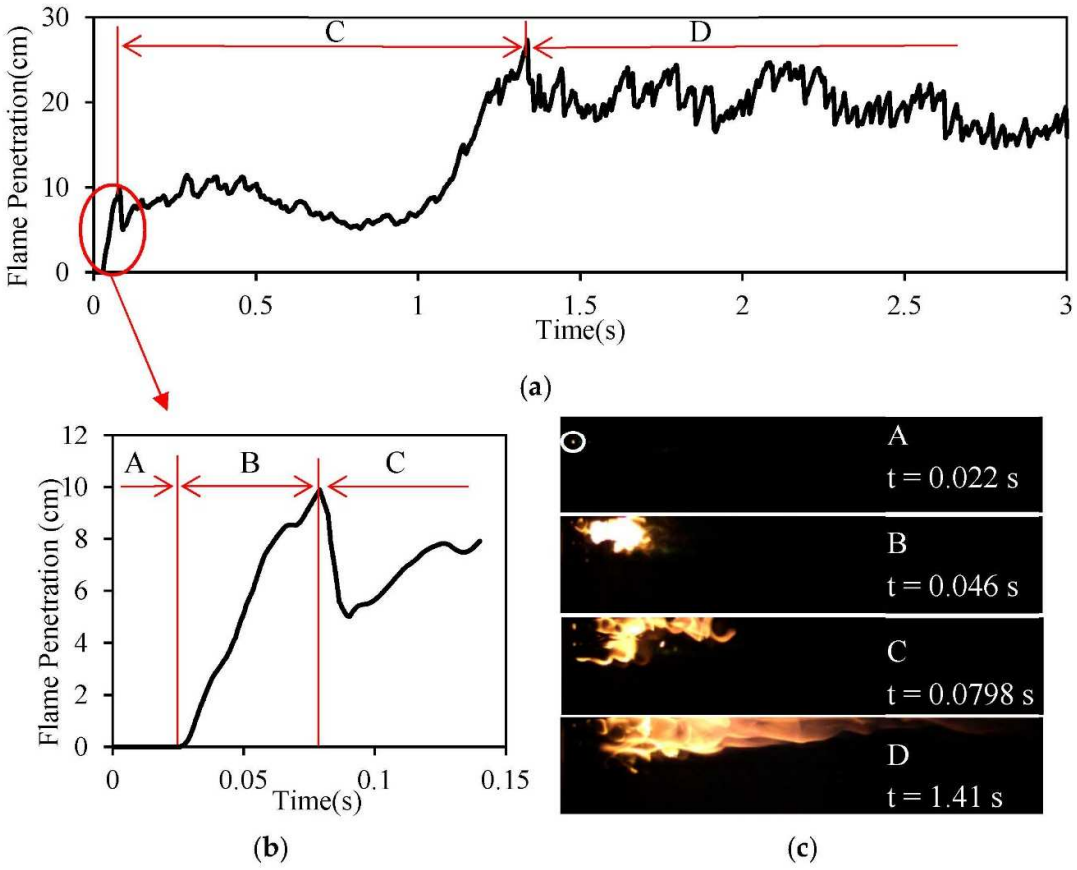

Figure 3. (**a**) Flame penetration, (**b**) local flame penetration magnification chart and (**c**) flame images with the air flow velocity of 1.4 m/s in the combustion chamber under the diesel flow rate of 10.0 mL/min.

The morphology of the combustion process is shown in Figure 3c. The start time of stage A was defined as 0 s. The flame inside the intake manifold burner was shown through the holes of the flame shroud at 0.022 s, as denoted by a white dotted circle. Then, the flame rushed out from the intake manifold burner into the combustion chamber, forming a near-linear development of flame penetration, namely, stage B. After a while with continuous fluctuations, namely, stage C, the flame finally reached the longest penetration and fluctuated around 18–25 cm (stage D).

4.2.1. Effect of Diesel Flow Rate on the Flame Penetration

The combustion processes under the diesel flow rate of 10.0 mL/min and 15.2 mL/min were shown in Figures 4 and 5. When the liquid diesel was injected into the intake manifold burner, it was evaporated and blown away by the cross wind, leading to the delay of ignition and flame development. During stage A, the flame could be seen through the holes in the flame shroud, as shown at 0.002 s in Figure 4 and 0.0534 s in Figure 5.

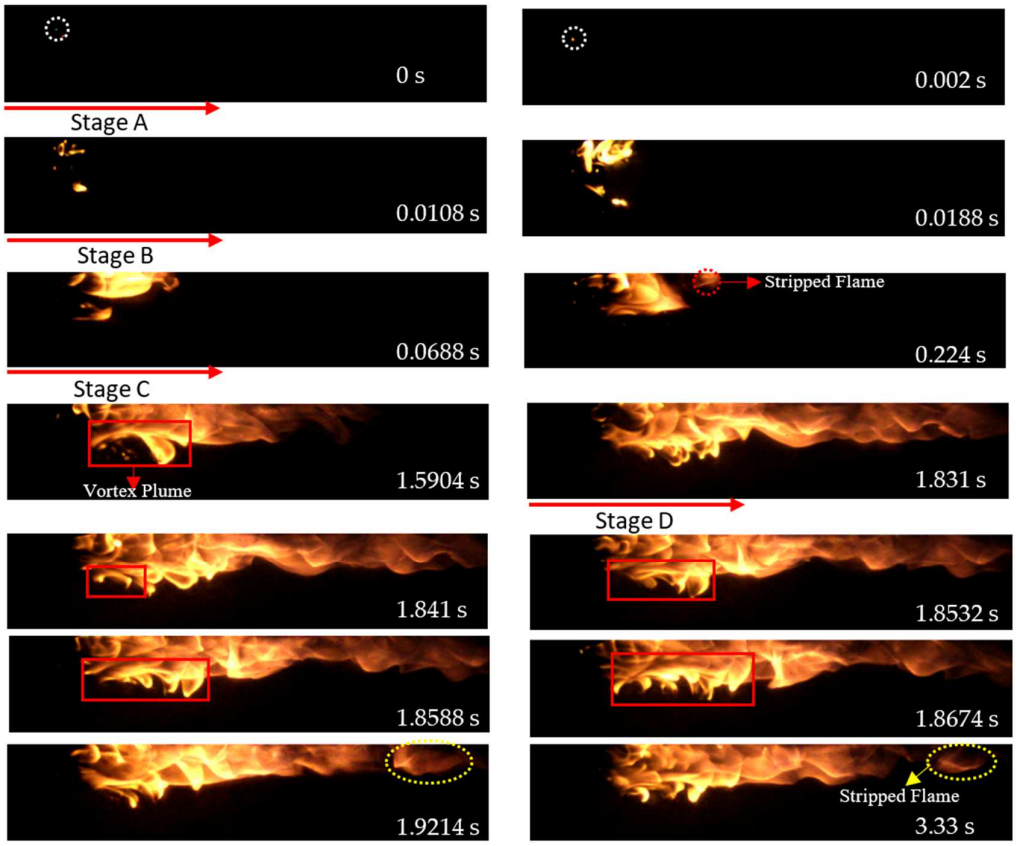

Figure 4. Flame propagation under the air flow velocity of 1.4 m/s and the diesel flow rate of 10.0 mL/min.

The flame stripping was captured in the steady-development stage C and stable stage D, as denoted by the red and yellow dotted circles, respectively. After stripping from the main flame, the flame burned itself quickly and disappeared. Stripped flames in stages C and D were found under all the test conditions in the present study (with the diesel flow rate ranging from 7.3 mL/min to 18.9 mL/min). Flame stripping is a common phenomenon at the steady-development stage and stable stage, leading to the abrupt decrease in flame penetration and area. Compared with stage D, the stripped flame in stage C showed higher brightness, indicating that more unburnt fuel existed in the packets. The stripped flame in stage D had less unburnt fuel because the fuel-air mixture was consumed by the combustion process.

The outer shell of the intake manifold burner had a high temperature due to the heat conduction from the heating elements. Thus, as shown by a red dashed rectangle in Figure 6, the downstream zone close to the intake manifold burner had a lower velocity and smaller density, leading to vortex formation due to the thermal buoyancy and air motion. As shown in the red rectangle in Figures 4 and 5, when the flame developed out from the intake manifold burner, the vortex structure of the flame, which is named the "vortex plume", was captured downstream close to the intake manifold burner. As time elapsed, the vortex developed along the air flow direction to the whole combustion chamber, leading to the flame rolling over and flame stripping.

When the diesel flow rate was 15.2 mL/min, the vortex generated in the same region as 10.0 mL/min. Then the vortex developed along the direction of air flow to the whole flame and became unclear to distinguish. The occurrence probability of flame stripping was similar under different diesel flow rates, indicating that the diesel flow was irrelevant to the flame motion.

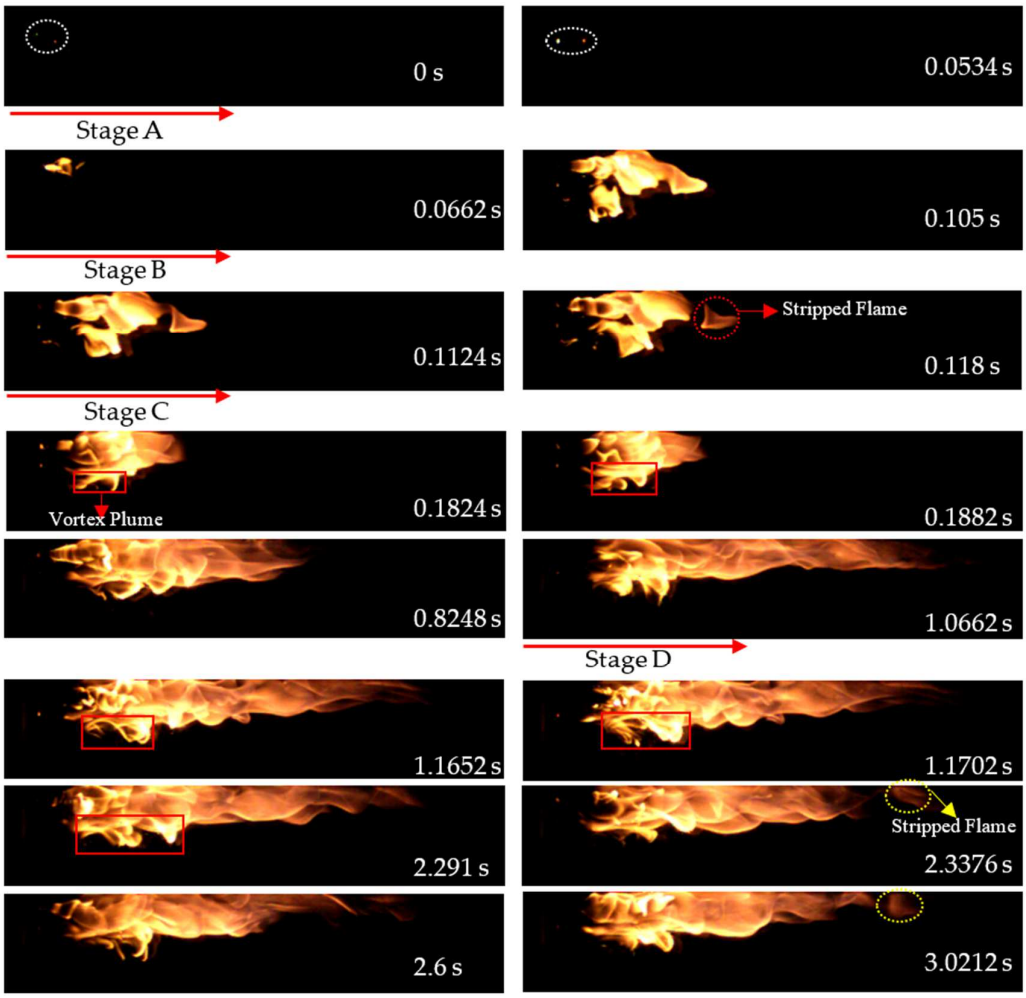

Figure 5. Flame propagation under the air flow velocity of 1.4 m/s and the diesel flow rate of 15.2 mL/min.

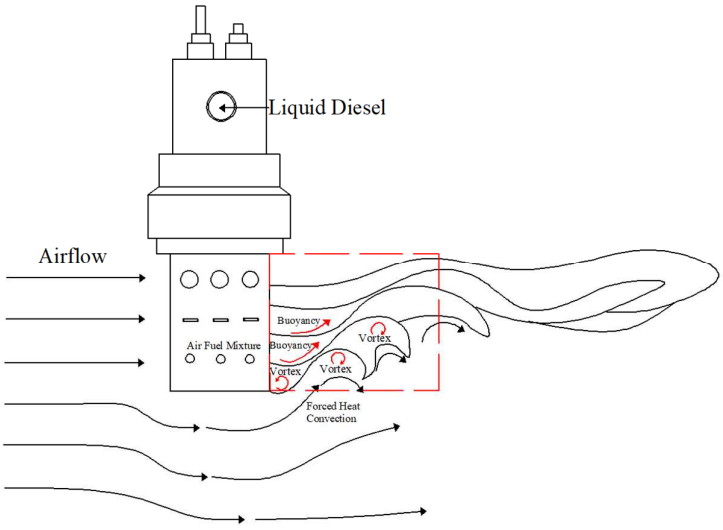

Figure 6. The physics of burner flame.

Image processing is shown in Figure 7a. The threshold of 0.12 for the in-house built MATLAB script was employed and the flame was identified due to the significant difference between the flame and background. Then, the flame penetration and area were calculated through the binary images. The flame penetration was defined as the distance between the

flame tip and the intake manifold burner, as shown in Figure 7a. The flame penetration under different diesel flow rates is shown in Figure 7b. The delay time was random in stage A. Thus, only stages B, C, and D are plotted in the next sections. As seen from the figures, the flame penetration and flame area performed a fluctuation waveform in stage C. With the diesel flow rate increasing from 7.3 mL/min to 13.0 mL/min, the flame area and penetration in stage D increased, indicating that the combustion was boosted. When the flow exceeded 14.5 mL/min, the value in stage D stayed nearly the same with the increasing flow rate, meaning that the promoting effect of the fuel flow rate had reached the limit.

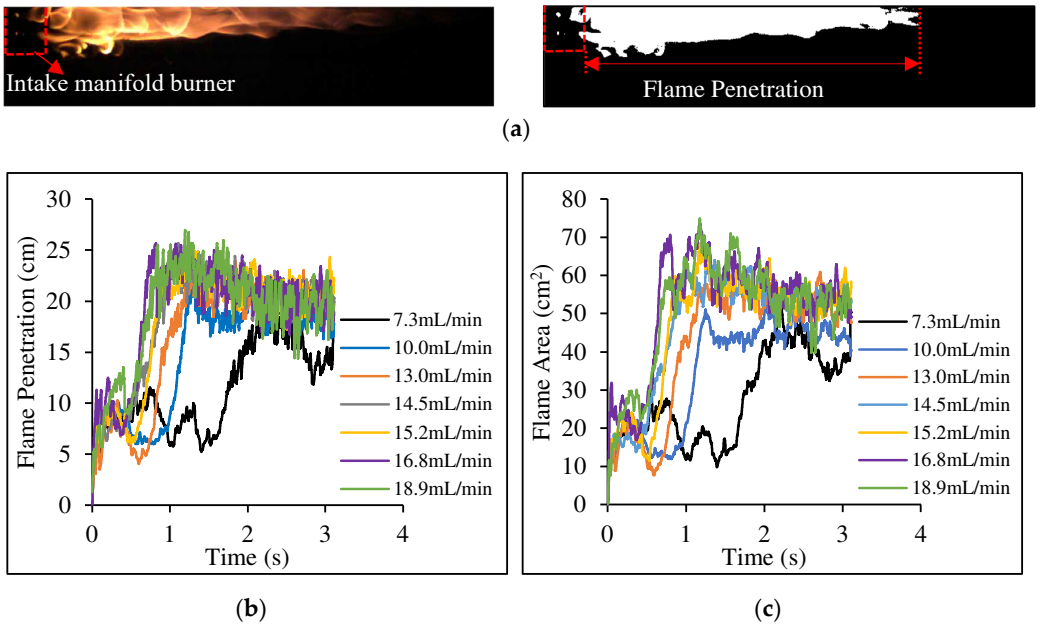

Figure 7. (**a**) Image processing; (**b**) flame penetration, and (**c**) flame area under different diesel flow rates with the air flow velocity of 1.4 m/s.

4.2.2. Effect of Intake Air Flow velocity on the Flame Penetration

The flame stripping was studied with the air flow velocity ranging from 1.4 m/s to 3.0 m/s. As the air flow velocity ranged from 2.0 m/s to 3.0 m/s, flame stripping in stage D was found in all the experiments. However, the flame stripping showed an occurrence probability lower than 100% under 1.4 m/s and 1.8 m/s.

Generally, the stripped flames under higher air flow velocity from 2.0 m/s to 3.0 m/s showed higher brightness due to the relatively higher amount of unburnt fuel in the packet, for instance, at 1.545 s and 1.56 s, as shown in Figure 8. The dimer stripped flames, for instance at 1.102 s and 1.26 s under 2.5 m/s, showed a lower occurrence probability. Under high air flow velocity, stripped flames often appeared, as shown in 1.114 s, 1.2552 s, 1.26 s and 1.56 s in Figure 8. Two continuously stripped flames were shown at 1.545 s, which is a rare phenomenon under high air flow velocity due to the strong flame vortex caused by the cross wind.

During stage D, it can be drawn from the figures that the stripped flames under 2.5 m/s were overall brighter than those under 1.4 m/s due to the boosted air motion. The stripped flames in stage D under low air flow velocity with 1.4 m/s and 1.8 m/s were dim and disappeared quickly due to the low amount of unburnt fuel entrained in the packet. Under the low air flow velocity of 1.4 m/s, the amount of stripped flames in both stage C and stage D was much less than that under higher air flow velocity (2.5 m/s) due to the milder combustion process, air motion, and better stability. Air motion was strengthened by the high air flow velocity, forming stronger vortexes. Therefore, the flame rolled and rotated more violently, leading to more stripped flames with more unburnt fuel entraining in the packet.

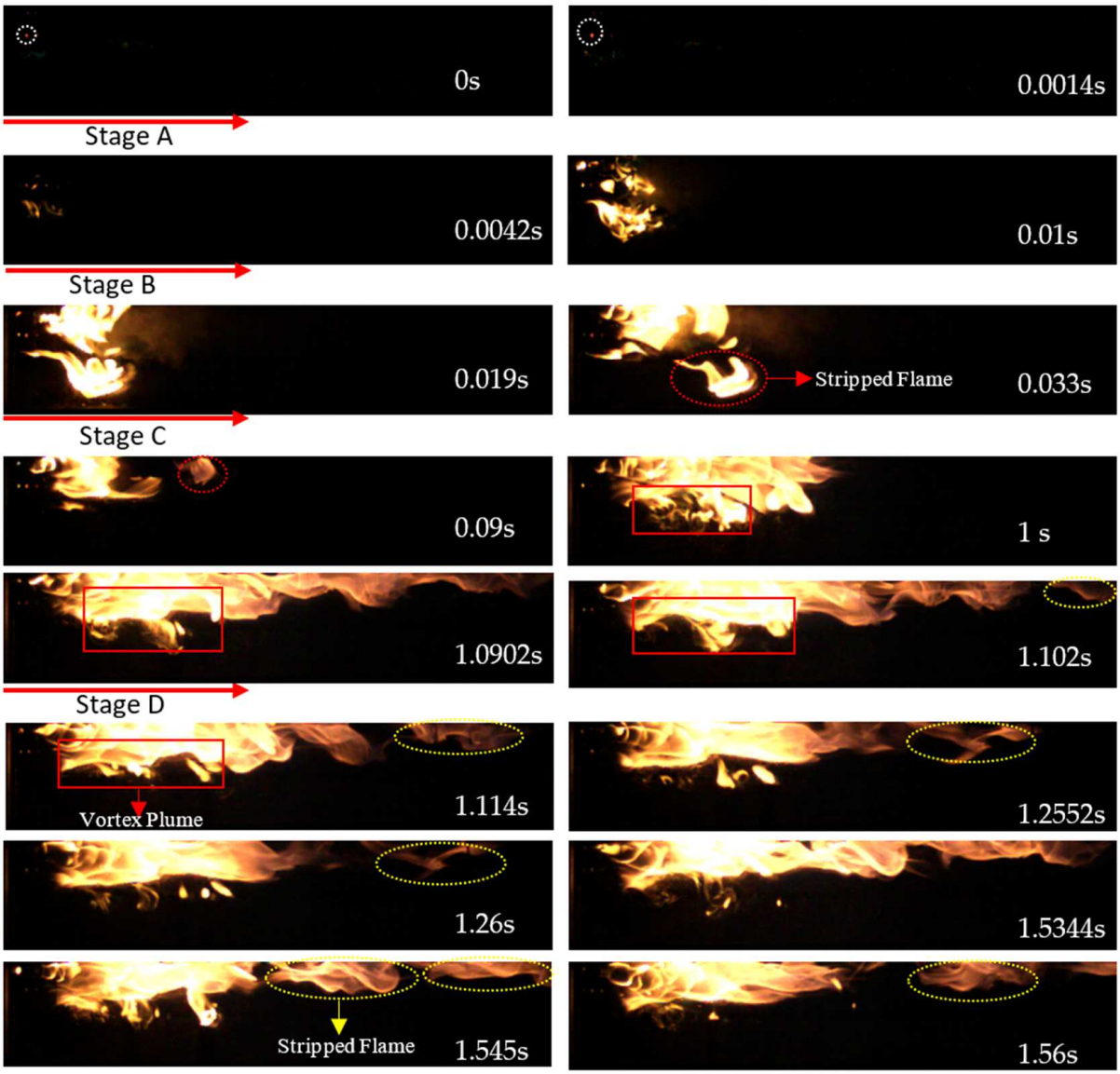

Figure 8. Flame propagation under the air flow velocity of 2.5 m/s and the diesel flow rate of 10.0 mL/min.

The results of flame penetration under different air flow velocities are shown in Figure 9. In all the cases within the air flow velocity of 2.6 m/s, stage C performed a fluctuation growth process. The maximum flame penetrations under different air flow were almost the same. During the process before ignition, the actual temperature rise in the combustion chamber was extremely small and negligible. The downstream zone close to the intake manifold burner showed a slight temperature rise during stage A. Therefore, when the flame rushed out, the flame was unstable due to the low temperature in the combustion chamber. It took a short duration within 2 s; that is to say, the duration of stage C to heat the air and metal shroud. Then, the flame developed to the longest penetration and entered the stable stage. At low air flow velocity, the fluctuation in stage D was chaotic and the varying amplitude was small. The fluctuations became more regular and with larger varying amplitude when the air flow velocity increased, indicating that the stronger cross wind enhanced the flame motion and led to more flame stripping. The error bar under the air flow velocity of 1.8 m/s and the diesel flow rate of 10.0 mL/min is shown in Figure 9b, indicating the good repeatability.

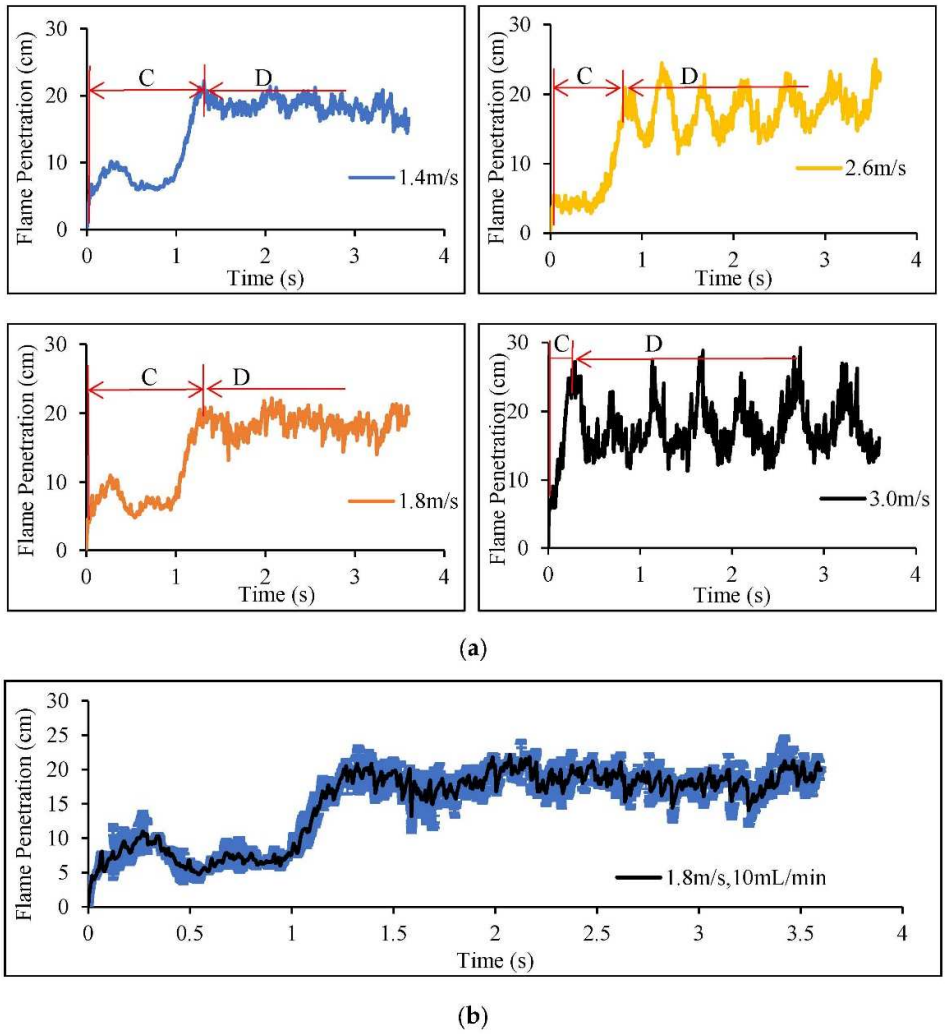

Figure 9. (**a**) Flame penetration under different air flow velocities with the diesel flow rate of 10.0 mL/min and (**b**) the error bar under 1.8 m/s.

4.3. Combustion Instability

The instability of combustion was calculated by the flame area in the period of stage D, as shown below:

$$\text{Instability} = \sqrt{\frac{\sum_{i=1}^{n}(x_i - \overline{x})^2}{n-1}} / \overline{x} \quad (3)$$

The combustion instability under different diesel flow rates and different air flow velocities are shown in Figure 10. It is seen that as the diesel flow rate increased, the combustion instability firstly decreased then increased. With the increase in diesel flow rate from 7.3 mL/min to 13.0 mL/min, more diesel was evaporated, leading to a higher gaseous diesel concentration in the flame shroud. Therefore, the combustion was boosted and the corresponding flame penetration increased, leading to higher heat release. The proportion of the forced convection of wind decreased, leading to lower instability. However, as the fuel flow rate increased from 14.5 mL/min to 18.9 mL/min, the diesel evaporation capacity of the heating elements had reached the limit due to the fixed heating area and power supply. Therefore, the flame penetration stayed nearly the same and excessive fuel made the fuel evaporation incomplete, leading to incomplete combustion. Additionally, compared with gaseous diesel, the non-evaporated liquid diesel took away more heat from the heating elements, causing the cooling of the heating rods and diesel evaporation deterioration. Moreover, the liquid diesel made the mixture of air and gaseous diesel nonuniform which further deteriorated the combustion. Therefore, the combustion instability increased with

the increasing fuel flow rate from 14.5 mL/min to 18.9 mL/min, and the fuel flow rate of 14.5 mL/min was the optimum value.

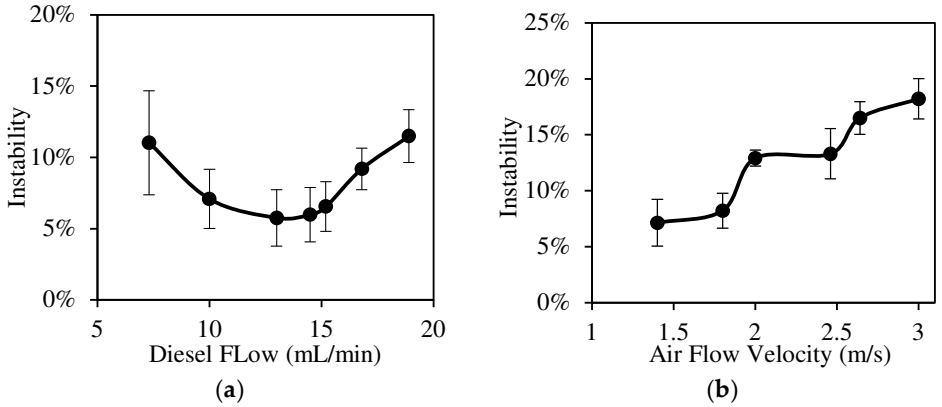

Figure 10. The instability of combustion under (**a**) different diesel flow rates and (**b**) air flow velocities.

As the air flow velocity increased from 1.4 m/s to 3.0 m/s, the combustion process was promoted by the increased oxygen concentration. More heat was carried away by the cross wind due to the increasing forced convection. Quicker fuel consumption was found at the tail of the flame plume. With the increase in air flow velocity, the vortex in the combustion chamber was strengthened. Therefore, more flame was stripped from the main flame, leading to higher instability. The flame penetration in stage D showed no significant difference but the more violent periodic pulsation with the increased air flow velocity from 1.4 m/s to 3.0 m/s. Higher flame area and brighter flame lightness was shown under 1.8 m/s compared with that under 1.4 m/s. Thus, 1.8 m/s was the optimum value for the air flow velocity.

4.4. Preheating Effect of the Intake Manifold Burner

The preheating effect of the intake manifold burner was evaluated by the temperature rise of the air flow. In order to get the preheating effect of the combustion, thermocouples were installed on the exhaust pipe with the distance of 420 mm, 488 mm, 550 mm, 655 mm, 775 mm, 925 mm, and 1120 mm away from the intake manifold burner, respectively. The temperature rise in the exhaust pipe under the air flow velocity of 2.0 m/s is shown in Figure 11.

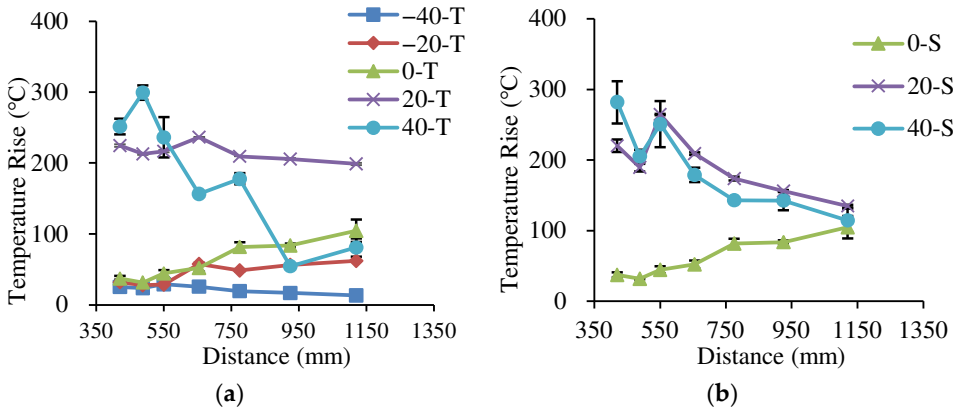

Figure 11. The temperature rise of (**a**) the vertical and (**b**) horizon axis in the exhaust pipe under the fuel flow rate of 10.0 mL/min with the air flow velocity of 2.0 m/s.

In the vertical plane, with the distance of 420 mm and 488 mm away from the intake manifold burner, the temperature rise at 40 mm was much higher than that at 20 mm, −20 mm, and 0 mm. Then, the temperature rise curve shows an overall declining trend

along the air flow direction, gradually approaching the temperature at 20 mm with the distance of 550 mm and getting much lower until 925 mm because the heat at 40 mm transferred downward. The air at 20 mm absorbed the heat from 40 mm and transferred heat to 0 mm, leading to a complex curve within 655 mm. When the distance exceeded 655 mm, the heat absorbed from 40 mm was lower than that transferred out, leading to the decreasing temperature rise at 20 mm. Therefore, though accompanied by some fluctuations, the temperature rise at 20 mm stayed at a relatively high value. The temperature rise at −40 mm, −20 mm, and 0 mm was much lower than that at 40 mm and 20 mm within 775 mm away from the intake manifold burner, meaning that the warm air that flowed out from the combustion chamber was mainly distributed in the zone near the upper wall due to the thermal buoyancy. With the increasing distance away from the intake manifold burner, the temperature at −20 mm and 0 mm showed an increasing trend, indicating the heat transfers from the upper zone to the central region. The temperature rise at −40 mm showed the lowest value in the vertical axis. The heat in the upper zone mainly transferred to the central region and there was not much left at −40 mm. Thus, the heat at −40 mm was easy to dissipate, leading to a decreasing trend from 655 mm to 1120 mm.

As described above, it can be drawn from the temperature distribution that the warm air concentrates in the upper region of the pipe first then moves downward from the upper wall to the pipe center and transfers the heat to the cold air. Along the direction of the pipe axis, the difference of temperature rise in the cross-section decreases, leading to more uniform heat energy distribution with the increasing distance. Different from the heat concentration in the region close to the upper part in the vertical axis, the heat energy in the horizon axis concentrates in the two sides close to the pipe wall. The intake manifold burner consisted of two heating elements, leading to the heat concentrating in the two sides close to the combustion chamber wall. Thus, the temperature rise at 40 mm and 20 mm was much higher than that at 0 mm. As the distance increased, the temperature rise showed an increasing trend at 0 mm while a completely different downward trend was shown at 40 mm and 20 mm, indicating that the heat transferred from regions near the pipe wall to the central zone.

The temperature rise under different fuel flow rates with the air flow velocity of 10.0 m/s is shown in Figure 12. With the increasing distance from the intake manifold burner, the temperature rise of the vertical axis showed an overall decreasing trend because more heat was carried away by the high-speed air flow.

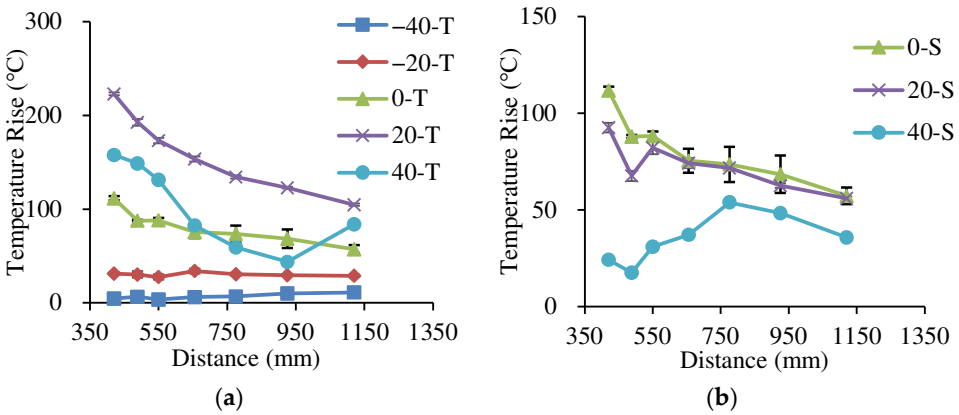

Figure 12. The temperature rise of (**a**) the vertical and (**b**) horizon axis in the exhaust pipe under the fuel flow rate of 10.0 mL/min with the air flow velocity of 10.0 m/s.

The heat distribution under the air flow of 10.0 m/s showed an entirely different distribution with that under 2.0 m/s. In the vertical plane, the temperature rise difference between the adjacent points was smaller under 10.0 m/s, indicating a more uniform heat distribution. The point at 20 mm under the air flow velocity of 10.0 m/s showed the highest temperature, indicating that the warm air flow was mainly distributed in the center of the

upper region. The temperature rise at −20 mm and −40 mm was much more stable than that under 2.0 m/s, indicating the heat transferred from the upper and central zones was much less than that under low-speed air flow. Thus, the preheating effect of burner flame on the lower zone close to the pipe wall could be ignored.

In the horizon plane, the temperature rise at 20 mm and 0 mm was much higher than that at 40 mm, indicating that the warm air mainly gathered in the central region of the pipe. The temperature rise at the horizon axis was lower compared with that at the vertical axis, meaning that the warm air mainly gathered in the upper region of the pipe due to the thermal buoyancy effect. The temperature distribution at both the vertical and horizon axis gradually converged with the increasing distance, indicating a more uniform heat distribution along the pipe. The temperature rise between the adjacent positions under 10.0 m/s was much closer than that under 2.0 m/s, showing better uniformity. This suggested that high-speed air flow accelerated the heat convection.

The average temperature rise and the combustion efficiency under different fuel flow rates are shown in Figure 13. The specific heat capacity of the exhaust gas was calculated through the equation shown below:

$$c = \sum g_i * c_i \quad (4)$$

where g_i is the mass percentage of each component and c_i is the corresponding specific heat capacity. This paper assumed that the liquid fuel combusts completely and is converted to CO_2 and H_2O. Thus, the specific heat capacity of the exhaust gas was calculated through the mixture of air, CO_2, and H_2O. Then, the combustion efficiency was obtained. Though minor inaccuracy (within 3.9%) of the specific heat capacity was introduced, the error was negligible. The combustion efficiency was calculated by the following equation:

$$\eta = (cm\Delta t + Q_3)/(Q_1 + Q_2) \quad (5)$$

where Q_1 and Q_2 are the heat of diesel and heating rods, respectively. Q_3 is the heat loss along the exhaust pipe, m is the mass flow rate of the intake air, and Δt is the average temperature rise in the cross section.

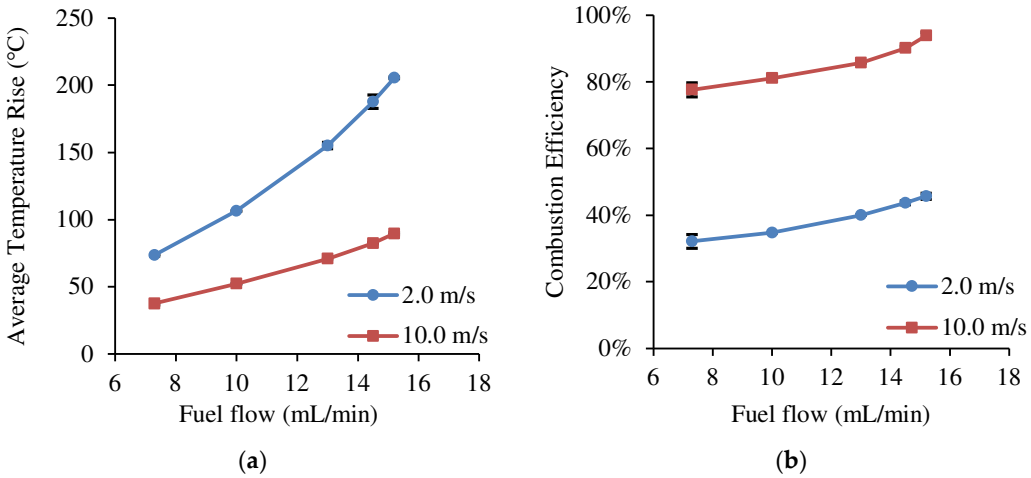

Figure 13. (**a**) The average temperature rise and (**b**) the combustion efficiency in the exhaust pipe with the air flow velocity of 2.0 m/s and 10.0 m/s.

As described above, the temperature distribution becomes more uniform along the pipe. Therefore, the temperature rise at the distance of 1120 mm away from the intake manifold burner was used to calculate the combustion efficiency. The average temperature rise increased with the increasing diesel flow rate, leading to higher combustion efficiency. With the increase in the diesel flow rate from 7.3 mL/min to 13.0 mL/min, the promotion of the combustion process under 1.4 m/s was found through the increased flame penetration.

Thus, it can be concluded that the combustion was boosted by the increased diesel flow rate under the air flow of 1.4 m/s, 2.0 m/s, and 10.0 m/s. Compared with the case under 2.0 m/s, though the average temperature rise under 10.0 m/s was lower due to more heat being carried away by the high-speed air flow, the corresponding combustion efficiency was higher.

5. Summary and Conclusions

5.1. Conclusions

The combustion process of the intake manifold burner was investigated through the high-speed visualization technique. In this study, the effects of diesel flow rate and air flow velocity on the combustion process and combustion efficiency were studied. The preheating effect on the intake air was also investigated through the temperature rise in the exhaust pipe. The following conclusions could be drawn.

1. The combustion process of the intake manifold burner showed four stages: preparing stage A, rapid development stage B, steady-development stage C, and stable stage D. Flame stripping was found in stage C and stage D due to the vortex in the combustion chamber.
2. Air flow showed a significant effect on flame motion while the effect of diesel flow was negligible. The vortex was enhanced under high air flow velocity, generally leading to more stripped flames with higher brightness compared with that under low air flow velocity.
3. The warm air concentrated in the upper region of the pipe first due to the thermal buoyancy, then the warm air moved downward. The warm air mainly gathered in the upper region of the pipe under 2.0 m/s while it mainly distributed in the center of the upper zone under 10.0 m/s.
4. Though a lower average temperature rise was shown under 10.0 m/s, the corresponding combustion efficiency was higher than that under 2.0 m/s. Stronger cross wind enhanced the heat convection, leading to better uniformity and more concentrated temperature distribution in the exhaust pipe.
5. Under the air flow velocity of 2.0 m/s and 10.0 m/s, the average temperature rise and combustion efficiency increased as the diesel flow rate increased. It could be seen that the combustion was enhanced with increasing diesel flow rate.

5.2. Recommendation

Concerning that the real intake air flow of the diesel engine fluctuates periodically, the authors recommend further investigations as follows:

1. Introduce the fluctuating intake air flow to replace the fixed air flow. Study the effect of the intake air flow fluctuation on the flame motion.
2. Expand the waveform of the fluctuating intake air flow, further investigating the frequency and amplitude impacts on combustion instability of the intake manifold burner.

Author Contributions: Conceptualization, Z.L. and Z.W.; methodology, Z.L.; formal analysis, Z.L.; investigation, Z.L. and H.M.; resources, H.W.; data curation, Z.L. and H.M.; writing—original draft preparation, Z.L.; writing—review and editing, Z.W.; visualization, Z.L.; supervision, Z.W.; project administration, Z.W. All authors have read and agreed to the published version of the manuscript.

Funding: This research was supported by National Natural Science Foundation of China (Grant No.: 51806012) and Beijing Natural Science Foundation (3192032).

Institutional Review Board Statement: Not applicable.

Informed Consent Statement: Not applicable.

Data Availability Statement: Not applicable.

Conflicts of Interest: The authors declare no conflict of interest.

References

1. O'Driscoll, R.; Stettler, M.E.J.; Molden, N.; Oxley, T.; ApSimon, H.M. Real world CO2 and NOx emissions from 149 Euro 5 and 6 diesel, gasoline and hybrid passenger cars. *Sci. Total Environ.* **2018**, *621*, 282–290. [CrossRef] [PubMed]
2. Wang, Z.M.; Ding, H.C.; Ma, X.; Xu, H.M.; Wyszynski, M.L. Ultra-high speed imaging study of the diesel spray close to the injector tip at the initial opening stage with split injection. *Appl. Energy* **2016**, *163*, 105–117. [CrossRef]
3. Martínez-Martínez, S.; de la Garza, O.A.; García-Yera, M.; Martínez-Carrillo, R.; Sánchez-Cruz, F.A. Hydraulic Interactions between Injection Events Using Multiple Injection Strategies and a Solenoid Diesel Injector. *Energies* **2021**, *14*, 3087. [CrossRef]
4. Zarrinkolah, M.T.; Hosseini, V. Detailed Analysis of the Effects of Biodiesel Fraction Increase on the Combustion Stability and Characteristics of a Reactivity-Controlled Compression Ignition Diesel-Biodiesel/Natural Gas Engine. *Energies* **2022**, *15*, 1094. [CrossRef]
5. Wang, Z.; Wu, S.; Huang, Y.; Chen, Y.; Shi, S.; Cheng, X.; Huang, R. Evaporation and ignition characteristics of water emulsified diesel under conventional and low temperature combustion conditions. *Energies* **2017**, *10*, 1109. [CrossRef]
6. Yi, W.; Liu, H.; Feng, L.; Wang, Y.; Cui, Y.; Liu, W.; Yao, M. Multiple optical diagnostics on effects of fuel properties on spray flames under oxygen-enriched conditions. *Fuel* **2021**, *291*, 120129. [CrossRef]
7. Henein, N.A.; Zahdeh, A.R.; Yassine, M.K.; Bryzik, W. Diesel engine cold starting: Combustion instability. *SAE Trans.* **1992**, *101*, 33–48.
8. Mann, N.; Joppig, P.; Sommer, H.; Sulzbacher, W. *Fuel Effects on the Low Temperature Performance of Two Generations of Mercedes-Benz Heavy-Duty Diesel Engines*; SAE Technical Paper 1999-01-3594; SAE International: Warrendale, PA, USA, 1999.
9. Ko, J.; Son, J.; Myung, C.-L.; Park, S. Comparative study on low ambient temperature regulated/unregulated emissions characteristics of idling light-duty diesel vehicles at cold start and hot restart. *Fuel* **2018**, *233*, 620–631. [CrossRef]
10. Bielaczyc, P.; Merkisz, J.; Pielecha, J. *Investigation of Exhaust Emissions from DI Diesel Engine During Cold and Warm Start*; SAE Technical Paper 2001-01-1260; SAE International: Warrendale, PA, USA, 2001.
11. Sakunthalai, R.A.; Xu, H.; Liu, D.; Tian, J.; Wyszynski, M.; Piaszyk, J. *Impact of Cold Ambient Conditions on Cold Start and Idle Emissions from Diesel Engines*; SAE Technical Paper 2014-01-2715; SAE International: Warrendale, PA, USA, 2014.
12. Liu, H.; Ma, S.; Zhang, Z.; Zheng, Z.; Yao, M. Study of the control strategies on soot reduction under early-injection conditions on a diesel engine. *Fuel* **2015**, *139*, 472–481. [CrossRef]
13. Roy, M.M.; Calder, J.; Wang, W.; Mangad, A.; Diniz, F.C.M. Cold start idle emissions from a modern Tier-4 turbo-charged diesel engine fueled with diesel-biodiesel, diesel-biodiesel-ethanol, and diesel-biodiesel-diethyl ether blends. *Appl. Energy* **2016**, *180*, 52–65. [CrossRef]
14. Zare, A.; Nabi, M.N.; Bodisco, T.A.; Hossain, F.M.; Rahman, M.M.; Van, T.C.; Ristovski, Z.D.; Brown, R.J. Diesel engine emissions with oxygenated fuels: A comparative study into cold-start and hot-start operation. *J. Clean. Prod.* **2017**, *162*, 997–1008. [CrossRef]
15. Park, H.; Bae, C.; Ha, C. A comprehensive analysis of multiple injection strategies for improving diesel combustion process under cold-start conditions. *Fuel* **2019**, *255*, 115762. [CrossRef]
16. Rath, M.K.; Acharya, S.K.; Patnaik, P.P. CI engine performance during cold weather condition using preheated air and engine by waste energy. *Int. J. Ambient Energy* **2016**, *38*, 534–540. [CrossRef]
17. Ramadhas, A.S.; Xu, H.M. Intake air heating strategy to reduce cold-start emissions from diesel engines. *Biofuels* **2018**, *9*, 405–414. [CrossRef]
18. Dardiotis, C.; Martini, G.; Marotta, A.; Manfredi, U. Low-temperature cold-start gaseous emissions of late technology passenger cars. *Appl. Energy* **2013**, *111*, 468–478. [CrossRef]
19. Pan, W.; Yao, C.; Han, G.; Wei, H.; Wang, Q. The impact of intake air temperature on performance and exhaust emissions of a diesel methanol dual fuel engine. *Fuel* **2015**, *162*, 101–110. [CrossRef]
20. Yontar, A.A.; Zhou, M.; Ahmad, S. Influence of intake air temperature control on characteristics of a Homogeneous Charge Compression Ignition engine for hydrogen-enriched kerosene-dimethyl ether usage. *Int. J. Hydrogen Energy* **2020**, *45*, 22019–22031. [CrossRef]
21. Broatch, A.; Ruiz, S.; Margot, X.; Gil, A. Methodology to estimate the threshold in-cylinder temperature for self-ignition of fuel during cold start of Diesel engines. *Energy* **2010**, *35*, 2251–2260. [CrossRef]
22. Li, Q.; Shayler, P.J.; McGhee, M.; La Rocca, A. The initiation and development of combustion under cold idling conditions using a glow plug in diesel engines. *Int. J. Engine Res.* **2017**, *18*, 240–255. [CrossRef]
23. Celik, A.; Yilmaz, M.; Yildiz, O.F. Effects of vortex tube on exhaust emissions during cold start of diesel engines. *Appl. Energy Combust. Sci.* **2021**, *6*, 100027. [CrossRef]
24. Celik, A.; Yilmaz, M.; Yildiz, O.F. Improvement of diesel engine startability under low temperatures by vortex tubes. *Energy Rep.* **2020**, *6*, 17–27. [CrossRef]
25. Deng, Y.; Liu, H.; Zhao, X.; Jiaqiang, E.; Chen, J. Effects of cold start control strategy on cold start performance of the diesel engine based on a comprehensive preheat diesel engine model. *Appl. Energy* **2018**, *210*, 279–287. [CrossRef]
26. Yilmaz, N. Effects of intake air preheat and fuel blend ratio on a diesel engine operating on biodiesel–methanol blends. *Fuel* **2012**, *94*, 444–447. [CrossRef]
27. Hákansson, N.O.; Kemlin, J.; Nilsson, R. Cold Starting the Volvo Way. *SAE Trans.* **1989**, *98*, 34–41.
28. Broatch, A.; Luján, J.M.; Serrano, J.R.; Pla, B. A procedure to reduce pollutant gases from Diesel combustion during European MVEG-A cycle by using electrical intake air-heaters. *Fuel* **2008**, *87*, 2760–2778. [CrossRef]

29. Payri, F.; Broatch, A.; Serrano, J.R.; Rodríguez, L.F.; Esmorís, A. Study of the potential of intake air heating in automotive DI diesel engines. *SAE Trans.* **2006**, *115*, 662–672.
30. Lindl, B.; Schmitz, H.-G. *Cold Start Equipment for Diesel Direct Injection Engines*; SAE Technical Paper 1999-01-1244; SAE International: Warrendale, PA, USA, 1999.
31. Isley, W. *Development of Multifuel Features of the LD-465 and LDS-465 Military Engines*; SAE Technical Paper No. 640371; SAE International: Warrendale, PA, USA, 1964.
32. Sun, R.; Sweet, E.J.; Zurio, J.; Zurlo, J.; Pfefferie, W.C.; Pfefferle, W.C. Diesel engine cold starting with catalytically ignited recirculated exhaust gas. *SAE Trans.* **1994**, *103*, 18–31.
33. Kreun, P.K.; Fajardo, C.M.; Baumann, A. Simulation of an Intake Manifold Preheater for Cold Engine Startup. *J. Eng. Gas Turbines Power* **2013**, *135*, 71505. [CrossRef]
34. Zhang, C.; Liu, B.; Hu, J.; Yu, X.; Wang, X. Study on cold starting performance of a low compression ratio diesel engine by using intake flame preheating. *Therm. Sci.* **2020**, *24*, 51–62. [CrossRef]